Atmos. Chem. Phys. Discuss., doi:10.5194/acp-2017-186, 2017
Manuscript under review for journal Atmos. Chem. Phys.
Discussion started: 7 March 2017

Atmospheric Chemistry and Physics Discussions

Multiphase composition changes and reactive oxygen species formation during limonene oxidation in the new Cambridge Atmospheric Simulation Chamber (CASC)

Peter J. Gallimore[1], Brendan M. Mahon[1], Francis P. H. Wragg[1], Stephen J. Fuller[1], Chiara Giorio[1,2], Ivan Kourtchev[1,3] and Markus Kalberer[1]

[1] Department of Chemistry, University of Cambridge, Lensfield Road, Cambridge, CB2 1EW, UK.
[2] now at Aix Marseille Université, CNRS, LCE UMR 7376, 13331 Marseille, France.
[3] now at Department of Chemistry, University College Cork, College Road, Cork, Ireland.

Correspondence to: Markus Kalberer (markus.kalberer@atm.ch.cam.ac.uk)

Abstract

The chemical composition of organic aerosols influences their impacts on human health and the climate system. Aerosol formation from gas-to-particle conversion and in-particle reaction was studied for the oxidation of limonene in a new facility, the Cambridge Atmospheric Simulation Chamber (CASC). Health-relevant oxidising organic species produced during SOA formation were quantified in real-time using an Online Particle-bound Reactive Oxygen Species Instrument (OPROSI). Two categories of reactive oxygen species (ROS) were identified based on time series analysis: a short-lived component produced during precursor ozonolysis with a lifetime on the order of minutes, and a stable component which was long-lived on the experiment timescale (~ 4 hours). Individual organic species were monitored continuously over this time using Extractive Electrospray Ionisation (EESI) Mass Spectrometry (MS) for the particle phase and Proton Transfer Reaction (PTR) MS for the gas phase. Many first generation oxidation products are unsaturated, and we observed multiphase aging via further ozonolysis reactions. Volatile products such as $C_9H_{14}O$ (limonaketone) and $C_{10}H_{16}O_2$ (limonaldehyde) were observed in the gas phase early in the experiment, before reacting again with ozone. Loss of $C_{10}H_{16}O_4$ (7-hydroxy limononic acid) from the particle phase was surprisingly slow. A combination of reduced C=C reactivity and viscous particle formation (relative to other SOA systems) may explain this, and both

Atmos. Chem. Phys. Discuss., doi:10.5194/acp-2017-186, 2017
Manuscript under review for journal Atmos. Chem. Phys.
Discussion started: 7 March 2017

scenarios were tested in the Pretty Good Aerosol Model (PG-AM). A range of characterisation measurements were also carried out to benchmark the chamber against existing facilities. This work demonstrates the utility of the CASC chamber, particularly for understanding the reactivity and health-relevant properties of organic aerosols using novel, highly time-resolved techniques.

1 Introduction

Organic aerosols make an important but poorly understood contribution to the climate system (Boucher et al., 2013). Airborne particles are also closely linked to the negative health effects of air pollution (Pope et al., 2009). Their atmospheric properties, including their interaction with trace gases and ability to act as cloud condensation nuclei, are closely linked to their chemical composition (Abbatt et al., 2012; Hallquist et al., 2009). Detailed chemical speciation is an important step towards understanding the formation and properties of aerosols. In particular, specific compound classes may dominate in certain processes. For example, water-soluble carbonyls may be responsible for a large fraction of aqueous secondary organic aerosol (SOA) formation (Ervens et al., 2011; McNeill et al., 2012). Similarly, organic reactive oxygen species (ROS), including organic peroxides and oxygen-centred radicals, are thought to be associated with the observed negative health effects of airborne particles (Verma et al., 2009).

SOA formation is an inherently multiphase process involving both gas-to-particle conversion and heterogeneous and in-particle chemistry (Kroll and Seinfeld, 2008). Atmospheric chambers constitute an invaluable tool for studying these processes under controlled conditions and relevant timescales. A variety of environmental chambers are in use globally, e.g. (Cocker et al., 2001; Hildebrandt et al., 2009; Klotz et al., 1998; Paulsen et al., 2005; Rohrer et al., 2004; Wang et al., 2014) to understand different aspects of atmospheric chemistry, air pollution and chemistry-climate interactions. Previous chamber studies have led to the discovery of important SOA formation and aging processes (Ehn et al., 2014; Kalberer et al., 2004; Odum et al., 1997; Shiraiwa et al., 2013).

Atmos. Chem. Phys. Discuss., doi:10.5194/acp-2017-186, 2017
Manuscript under review for journal Atmos. Chem. Phys.
Discussion started: 7 March 2017

Atmospheric Chemistry and Physics Discussions

The largest global source of SOA is from the oxidation of biogenic volatile organic compounds (BVOCs) (Hallquist et al., 2009). Limonene is a BVOC emitted in significant quantities (Guenther et al., 2000) in the biosphere. Its widespread use in industrial processes and household cleaning and fragrance products also results in elevated indoor concentrations with contingent impacts on indoor air quality (Wainman et al., 2000; Waring, 2016; Weschler and Shields, 1999). Limonene contains two reactive C=C double bonds which results in multiple generations of oxidation products (Bateman et al., 2009; Kundu et al., 2012; Walser et al., 2008) and high aerosol yields relative to other terpenes (Hoffmann et al., 1997). The endo C=C is more susceptible to ozonolysis by a factor of 10-50 (Zhang et al., 2006) and some of the first-generation ring opening products are condensable (Figure 1). Subsequent oxidation of the remaining double bond may therefore occur in either the gas or condensed phases depending on the properties of the initial products and the aerosol loading.

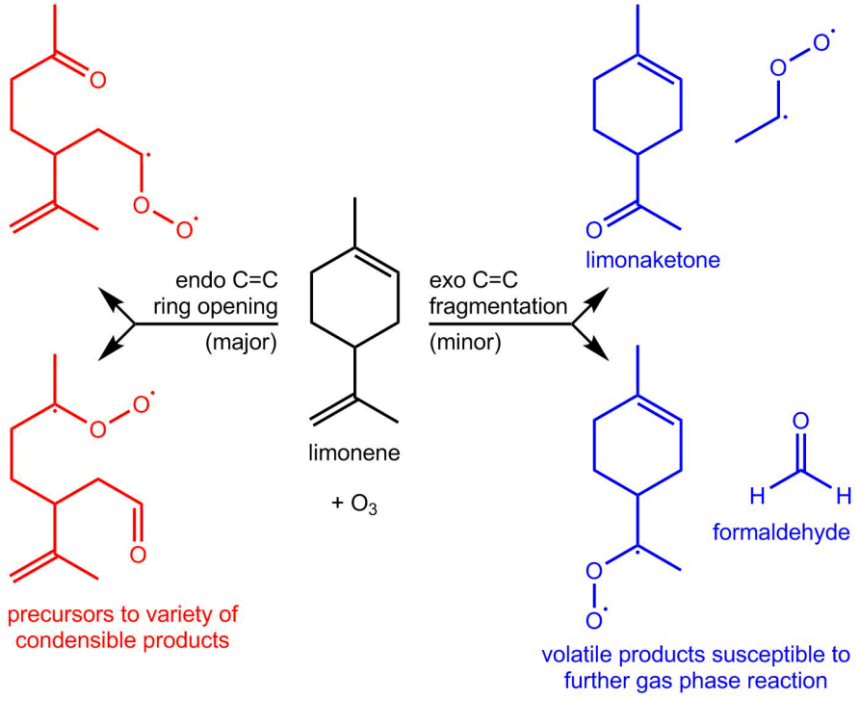

Figure 1: Initial products of limonene ozonolysis following reaction with the cyclic endo C=C (red channel) and terminal exo C=C (blue channel). The Criegee intermediates produced in these reactions can proceed to form a variety of multifunctional products observed both in the gas and particle phases.

Atmos. Chem. Phys. Discuss., doi:10.5194/acp-2017-186, 2017
Manuscript under review for journal Atmos. Chem. Phys.
Discussion started: 7 March 2017

Atmospheric Chemistry and Physics Discussions

The multiphase ozone-initiated oxidation of limonene to form SOA is studied in a new, state-of-the-art facility: The Cambridge Atmospheric Simulation Chamber (CASC). CASC is a 5.4 m^3 FEP chamber which is coupled to a range of unique online chemical characterisation instruments. An Extractive Electrospray Ionisation Mass Spectrometer (EESI-MS) provides real-time measurements of particle-phase molecular composition (Gallimore and Kalberer, 2013; Gallimore et al., submitted). Gas-phase VOC components are monitored using Proton Transfer Reaction Time of Flight (PTR-ToF) MS. Together these complementary techniques produce a detailed, highly time-resolved picture of the evolving organic components in the chamber on a molecular level. In parallel, an Online Particle-bound Reactive Oxygen Species Instrument (OPROSI) (Wragg et al., 2016) allows the health-relevant oxidising capacity of organic species to be quantified with high time resolution.

In our limonene ozonolysis experiments, we observe several reaction pathways using these instruments which contribute to SOA formation. These include: further oxidation of volatile unsaturated products in the gas phase, heterogeneous reaction of ozone with condensed double bonds, and reactive uptake of carbonyls to form accretion products. Most of the reactive chemistry is complete once the limonene has been consumed, but heterogeneous reaction and decomposition of ROS appear to continue on longer timescales. We develop model test cases and find that such apparently "slow" rates of change may be explained by a combination of inhibited diffusion within viscous particles and reduced reactivity compared to other SOA systems. Compared to the widely used SOA surrogate, oleic acid aerosol, limonene SOA exhibits a longer ROS lifetime and higher overall ROS yield which we rationalise in terms of their respective chemical characteristics.

2 Methodology

2.1 Chamber construction and operation

A schematic of the Cambridge Atmospheric Simulation Chamber (CASC) is given in Figure 2. The design is based on a 5.4 m^3 (1.5 × 1.8 × 2.0 m) collapsible bag made from 125 µm DuPont Teflon fluorocarbon film (FEP type 500A, Foiltec GmbH, Germany). The panels are heat sealed and bonded with Teflon tape (Polyflon Technology Ltd, UK) at the edges and

Atmos. Chem. Phys. Discuss., doi:10.5194/acp-2017-186, 2017
Manuscript under review for journal Atmos. Chem. Phys.
Discussion started: 7 March 2017

Atmospheric Chemistry and Physics Discussions

corners of the chamber. The bag is suspended in an aluminium frame (Rexroth, Bosch, Germany) and entirely enclosed by aluminium sheeting and Perspex panels covered with aluminium tape to reflect light. Stainless steel ports containing ¼" and ½" stainless steel bulkheads (Swagelok, UK) are attached to each end of the chamber to enable introduction and sampling of air from the chamber. An initial application of the chamber is described in Kourtchev et al. (2016).

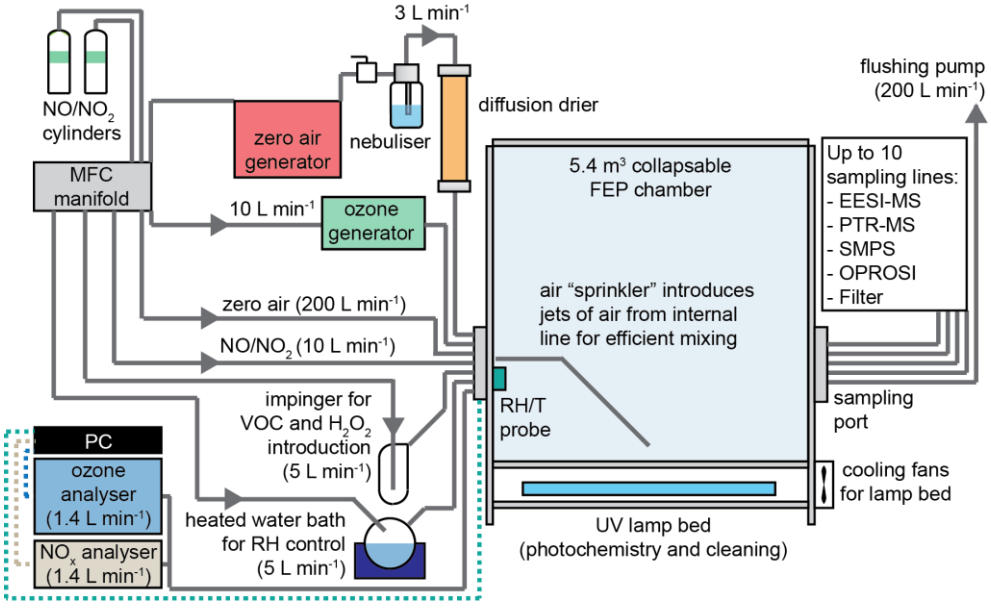

Figure 2: Schematic of the Cambridge Atmospheric Smog Chamber (CASC). The facility consists of a 5.4 m^3 collapsible FEP Teflon chamber with stainless steel ports at each end for introduction of gases and sampling of chamber air by a suite of instrumentation. Gas sampling lines are solid grey, data connections are dashed.

The temperature of the room which houses the chamber is controlled using a 7.1 kW air conditioning unit (Daikin, UK) and 10 fans are situated underneath one end of the chamber to circulate air from the room through the chamber enclosure. Light sources are situated under the bag and consist of twenty 160W UV tanning lamps (Philips Body Tone, > 300 nm) for use during photochemical aging experiments and four 75W "hard" UV lamps (Philips TUV75, 242 nm) for cleaning the chamber. The temperature in the chamber is typically 20 ±

Atmos. Chem. Phys. Discuss., doi:10.5194/acp-2017-186, 2017
Manuscript under review for journal Atmos. Chem. Phys.
Discussion started: 7 March 2017

1 °C for "dark" experiments and 24 ± 2 °C for photochemical aging experiments. Temperature is monitored along with relative humidity (RH) using a probe (Sensirion SHT75, UK) close to the inlet port of the chamber.

The chamber is filled with air from a zero air generator (KA-MT2, Parker Hannifin, UK). NO and NO_2 are supplied from cylinders (each 100 ppm, C grade, BOC, UK). Flow into the chamber is controlled through a series of mass flow controllers (MFCs) (MKS, UK). Water vapour is introduced by bubbling an air stream through a heated 0.5 L round-bottomed flask containing water (HPLC, Rathbones, UK). This process does not introduce detectable levels of particles or VOCs. Ozone is generated by flowing air through either an enclosed mercury UV lamp (Appleton Woods, UK) or a commercial ozone generator (LABOZONE09, ESCO International Ltd, UK). VOCs and aqueous H_2O_2 (if used) are introduced into separate glass impingers and evaporated using an air stream and heating from a heat gun (PHG 2, Bosch, Germany). Seed particles can be optionally introduced from an atomiser (Model 3076, TSI, UK) and are dried using a silica diffusion drier and neutralised with a Kr-85 source (Model 3077, TSI, UK) prior to introduction into the chamber.

A 200 L min^{-1} diaphragm pump (ET200, Charles Austen, UK) is used in combination with 200 L min^{-1} clean air introduction to flush the chamber. Flushing is carried out for at least 24 hours prior to the start of an experiment and may be accompanied by use of the "hard" UV lamps, ozone (~ 10 ppm) and water vapour to remove residual species from the chamber walls. The chamber is typically operated in a batch mode, where reactants are introduced into the chamber at the start of the experiment and allowed to evolve over a period of several hours. In principle it could also be operated in a flow-through mode, where continuous introduction of reactants produce steady state conditions in the chamber according to a characteristic mixing time.

2.2 Chamber instrumentation

A series of instruments used to monitor physical and chemical parameters of the chamber are listed in Table 1. In addition to a suite of commercially available instrumentation, we also

Atmos. Chem. Phys. Discuss., doi:10.5194/acp-2017-186, 2017
Manuscript under review for journal Atmos. Chem. Phys.
Discussion started: 7 March 2017

Atmospheric Chemistry and Physics Discussions

monitor the chemical evolution of the gas-phase and aerosols formed in the chamber using unique instruments developed in-house. Extractive Electrospray Ionisation Mass Spectrometery (EESI-MS) is an online particle analysis technique described in Gallimore and Kalberer (2013). It retains the key advantage of "soft" electrospray ionisation MS techniques, namely that quasi-molecular ions are produced from aerosol analytes with minimal fragmentation, and hence individual molecular species can be identified. It is also particularly suited to chamber measurements because time-resolved information is obtained and relative intensity changes can be linked to concentration changes in the particle Gallimore et al., (submitted).

Instrument	Measures	Range	Uncertainty	Time resolution
EESI-MS (Gallimore and Kalberer, 2013)	Particle-phase chemical composition	0.2-600 µg/m^3		4-6 minutes
OPROSI (Wragg et al., 2016)	Particle-bound reactive oxygen species (ROS)	0-2000 nmol [H_2O_2] equiv m^{-3}	2-4 nmol [H_2O_2] equiv m^{-3}	4 minutes
Ionicon PTR-ToF 8000 MS	Gas-phase VOCs			As low as 100 ms, typically 1 minute
TSI 3086 SMPS	Particle size distribution	14-700 nm		< 2.5 minutes
Thermo 49C ozone analyser	[O_3]	0-200 ppm	± 1 ppb up to 1 ppm	1 minute
Teledyne 200E NOx analyser	[NO], [NO2], [NOx]	0-1000 ppb	± 1 ppb	1 minute
Sensirion SHT75	RH, T	0-100% (RH), -40 – 120°C (T)	± 1.8% (RH), ± 0.3°C (T)	1 second

Table 1: Overview of CASC instrumentation. EESI-MS and OPROSI are unique instruments developed in-house.

The gas phase VOC composition of the chamber is monitored using Proton Transfer Reaction MS (Blake et al., 2009). The PTR-MS (PTR-ToF 8000, Ionicon, Innsbruck, Austria)

measures VOCs with a proton affinity higher than water in the *m/z* range 10-500, with a typical mass resolution of 5000 (full width at half maximum) at the mass of protonated acetone, and a typical time resolution of 1s. Typical detection limits are in the order of 1-2ppb at 1s time resolution and ~30ppt at 1min time resolution (Blake et al., 2009; de Gouw and Warneke, 2007). For these experiments, source settings were: drift tube voltage of 600 V, drift tube pressure at ~ 2.20 mbar, drift tube temperature at 60ºC, resulting in an E/N of ca. 135 Td (1 Td = 10^{-17} V cm^2). k = 2.54 × 10^{-9} cm^3 molecule^{-1} s^{-1} was used for limonene quantification (Zhao and Zhang, 2004) and a default rate constant (k) of 2 × 10^{-9} cm^3 molecule^{-1} s^{-1} was used for the other ions.

Reactive Oxygen Species (ROS) are associated with the negative health impacts of aerosols (den Hartigh et al., 2010; Steenhof et al., 2011). A new Online Particle-bound Reactive Oxygen Species Instrument (OPROSI), described in Wragg et al. (2016) is used to continuously monitor this health relevant property of aerosols from the chamber. OPROSI has a time resolution of 4 minutes (e-folding time during online particle collection tests) and is thus able to capture most time-dependant processes observed during SOA formation and evolution. This instrument is especially sensitive to short-lived ROS components, which react within seconds-minutes after sampling (see Wragg et al. (2016) for more details).

EESI-MS, PTR-MS and OPROSI are all placed in a laboratory just next the room that houses the chamber. Steel tubing (ca. 3 m length) connect the chamber with EESI-MS and OPROSI. The PTR-MS is connected via a 1mm inner diameter PTFE tube kept at room temperature.

2.3 Chamber photochemical characterisation

The tanning lamps used during photochemical aging experiments emit primarily in the range 300-400 nm (Figure S1(a)). Emissions below 300 nm, which in the atmosphere are attenuated before reaching the troposphere, are absent. This measured spectrum also overlaps with the absorption cross sections of NO_2 (λ < 400 nm) and to a small extent with O_3 (λ < 310 nm). Photolysis of these species drives photochemistry in the troposphere. By contrast, “black lamps”, which are commonly employed in chamber studies, emit over a narrower range, 350-

Atmos. Chem. Phys. Discuss., doi:10.5194/acp-2017-186, 2017
Manuscript under review for journal Atmos. Chem. Phys.
Discussion started: 7 March 2017

400 nm, where ozone photolysis will not occur. Transmission of light through the FEP film used for the bag was tested over the range 200-800 nm (Figure S1(b)). Transmission of light > 300 nm, used in aging experiments, was higher than 80 %. Transmission of "hard" UV from the cleaning lamps is also acceptable at > 60%.

The photolysis characteristics of the chamber were assessed by quantifying the photolysis frequency of NO_2, J_{NO2}. Following four NO_2 irradiation experiments in which the steady state concentrations of NO, NO_2 and O_3 were measured, J_{NO2} = 0.49 ± 0.09 min^{-1} was calculated (Table S1). This is within the range of values determined for other chambers and is comparable to ambient values in Pasadena, California (0.5 min^{-1}) (Cocker et al., 2001) and the outdoor EUPHORE chamber (0.44-0.56 min^{-1}) (Martın-Reviejo and Wirtz, 2005).

2.4 Mixing and wall losses

The chamber air volume is mixed using an "air sprinkler" system. High pressure air is introduced from a PTFE tube (4mm inner diameter) which extends from the introduction port across the entire the length of the chamber. Periodic holes along the tube allow "jets" of air to escape and mix the chamber volume. This approach avoids the use of mixing fans which may produce unwanted vapours or particles during operation. Mixing with and without use of the air sprinkler was assessed by evaporating α-pinene into the chamber and monitoring its concentration from the opposite port with the PTR-MS (Figure S2). With 3 × 10 s bursts from the air sprinkler over the course of a minute, the observed α-pinene concentration sampled at the far end of the chamber was seen to stabilise rapidly and reaches 90 % of its steady state value within 4 minutes of mixing. Without active mixing, the α-pinene concentration took around 30-40 minutes to reach a stable value. This efficient mixing procedure (adding ca. additional 100 L clean air into the chamber) is usually applied during the introduction of oxidants (for a "dark" experiment) or after the addition of all components, before initiating photochemistry (for photochemical aging experiments).

Atmos. Chem. Phys. Discuss., doi:10.5194/acp-2017-186, 2017
Manuscript under review for journal Atmos. Chem. Phys.
Discussion started: 7 March 2017

Atmospheric Chemistry and Physics Discussions

The loss of oxidants and VOCs to the walls of the chamber was tested using ozone and α-pinene as representative test species. Ozone was lost from the clean chamber at an average rate of 5.9×10^{-5} min^{-1} over 9 hours. This compares to a loss rate of 1.31×10^{-4} min^{-1} for a similar facility, described by Wang et al. (2014). During the α-pinene wall loss experiment, an average loss rate of 1.6×10^{-5} min^{-1} was observed over 14 hours.

Particle deposition to the chamber walls was also determined, assuming deposition to be a first order process (Cocker et al., 2001). Ten experiments involving the introduction of ammonium sulfate particles to the clean chamber were performed. Characteristic first-order coefficients for the rate of change of particle number and mass were found to be $\beta_N = 0.201 \pm 0.025$ h^{-1} and $\beta_M = 0.166 \pm 0.020$ h^{-1} respectively, as detailed in the supporting information. This corresponds to aerosol lifetimes of 5-6 hours, comparable to other chambers as illustrated in Table S2.

2.5 Aerosol numerical modelling

Illustrative model simulations were performed using the Pretty Good Aerosol Model (PG-AM). PG-AM is described in detail in Griffiths et al., (2009) and Gallimore et al., (submitted). In brief, the model treats the following processes: chemical reaction in both the gas and particle phases, gas-particle exchange via uptake and evaporation, and diffusion within the particle. Diffusion is parameterised according to Griffiths et al., (2009). The differential equations governing reaction and diffusion are integrated forwards in time using Mathematica (v11, Wolfram). In this study, loss of unsaturated $C_{10}H_{16}O_4$ from the particle by reaction with ozone was simulated for a single particle of characteristic radius $r_{eff} = 3V_t/S_t$ = 84 nm based on the measured total particle volume (V_t) and surface area (S_t). The bulk bimolecular rate constant for ozonolysis (k^{II}) and the ozone and organic diffusion coefficients (D_{O3} and D_{org}) were varied as described in the results. Ozone solubility ($K_{H,O3} = 0.1$ M atm^{-1}) (Morris et al., 2002) and accommodation ($\alpha_{O3} = 10^{-3}$) (Gallimore et al., submitted) were fixed based on the literature for oleic acid particles.

Atmos. Chem. Phys. Discuss., doi:10.5194/acp-2017-186, 2017
Manuscript under review for journal Atmos. Chem. Phys.
Discussion started: 7 March 2017

Atmospheric Chemistry and Physics Discussions

3. Limonene SOA formation and characterisation

Insight into the chemical and health-relevant properties of limonene-derived SOA is provided by the online characterisation techniques coupled to CASC. Before the introduction of reactants, the concentrations of O_3, NO_x and particles in the clean chamber were below the detection limits of the respective instruments in Table 1. The relative humidity of the chamber air was adjusted to 40 % and 6 µL limonene (> 99%, Sigma) was added and mixed to produce a starting concentration of ~190 ppb based on PTR-MS quantification. Ozone was introduced into the chamber over a 20 minute period, during which time the chamber air was regularly mixed; a maximum concentration of ~450 ppb was achieved. This corresponds to a stoichiometric excess of ozone with respect to the number of double bonds present in the limonene precursor.

SOA was produced rapidly following the introduction of ozone to the chamber (Figure 3). Particles grew via homogeneous nucleation into a single mode with diameter ~160 nm. The measured SMPS data (black curve) were corrected for particle wall losses (red curve) using a procedure similar to Rollins et al., (2009) which is described in the supplementary information. Over 85% of the loss-corrected mass was formed within the first 30 minutes of ozone introduction, with slower additional growth over the next ~ 3 hours of the experiment.

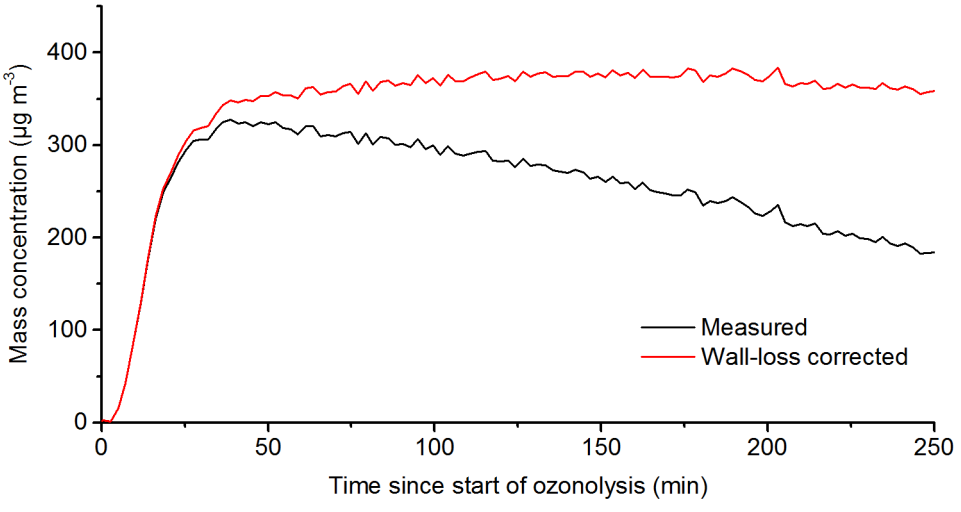

Atmos. Chem. Phys. Discuss., doi:10.5194/acp-2017-186, 2017
Manuscript under review for journal Atmos. Chem. Phys.
Discussion started: 7 March 2017

Atmospheric Chemistry and Physics Discussions

Figure 3: Time series showing evolution of the total SOA mass in the chamber (black curve). The measured concentration was corrected to account for particle deposition to the chamber walls (black curve).

3.1 Gas and particle molecular composition changes during ozonolysis

The characteristic time for limonene loss due to reaction with ozone was also 30 minutes (Figure 4). Limonene was quantified using PTR-ToF-MS from the sum of signals at *m/z* 137 ($[M + H]^+$) and *m/z* 81 (major fragment). We detect a number of gas-phase products, noting that structural isomers of the species described here cannot be distinguished in our analysis. These were mostly assigned as $[M + H]^+$ and agree well with previous studies of limonene and other terpene ozonolysis (Ishizuka et al., 2010; Lee et al., 2006). The largest yields are for ubiquitous small acids and carbonyls such as formic acid (*m/z* 47, Figure 4), formaldehyde (*m/z* 31, Figure 4), acetic acid, acetaldehyde and acetone. *m/z* 75 reported by Lee et al., (2006) is present here and based on our assigned neutral formula ($C_3H_6O_2$) could plausibly be propanoic acid, hydroxyacetone or methyl acetate.

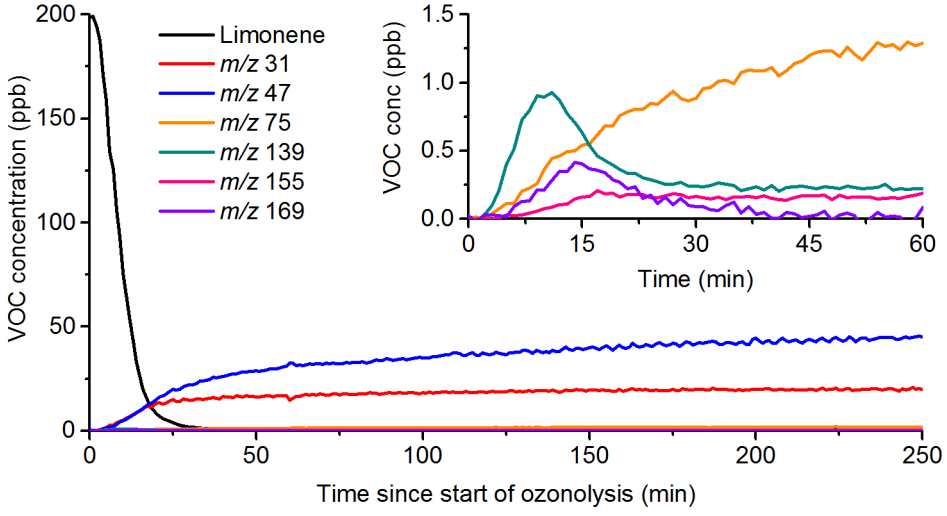

Figure 4: Concentrations of selected gas-phase VOCs including limonene, formaldehyde (*m/z* 31) and formic acid (*m/z* 47) detected using PTR-MS during limonene ozonolysis. The inset graph shows products formed in lower concentrations, including first-generation unsaturated species (*m/z* 139, limonaketone and *m/z* 169, limonaldehyde) which are removed by further ozonolysis.

Atmos. Chem. Phys. Discuss., doi:10.5194/acp-2017-186, 2017
Manuscript under review for journal Atmos. Chem. Phys.
Discussion started: 7 March 2017

Atmospheric Chemistry and Physics Discussions

Unsaturated gas-phase products corresponding to both reaction channels in Figure 1 can be detected at higher masses. In particular, limonaketone ($C_9H_{14}O$, *m/z* 139) is produced from the minor exo-ozonolysis channel and is the most volatile unsaturated product (Donahue et al., 2007). It peaks in concentration after 12 minutes before being depleted, presumably by oxidation of the remaining double bond in the gas phase. Relatively few products from the ring-opening endo C=C channel can be quantified, but we note that limononaldehyde ($C_{10}H_{16}O_2$, *m/z* 169), the analogous ring-opening product to limona ketone, exhibits a similar time dependence. Other products of endo C=C ozonolysis are generally condensable since a double functionalization reaction occurs without fragmenting the carbon backbone. Small gas phase signals for such products including *m/z* 155 ($C_9H_{14}O_2$) (Lee et al., 2006) (Figure 4), *m/z* 187 ($C_9H_{14}O_4$, limonic acid) and *m/z* 201 ($C_{10}H_{16}O_4$, 7-hydroxy limononic acid) were detected close to the instrument background.

We discuss these products further in the context of particle-phase composition measurements from EESI-MS, which is applied to long term (> 4 hour) SOA monitoring for the first time here. An EESI mass spectrum 50 minutes after the start of ozonolysis is shown in Figure 5(a). As for the PTR measurements, isobaric compounds may complicate interpretation of the spectrum. The ion source was operated in negative ionisation mode and the most abundant $[M - H]^-$ ions detected with EESI-MS compare well with previous offline ESI-MS studies (Bateman et al., 2009; Kundu et al., 2012; Walser et al., 2008). These include: *m/z* 185 (neutral formula $C_9H_{14}O_4$, limonic acid), *m/z* 171 ($C_8H_{12}O_4$, keto-limonalic acid), *m/z* 183 ($C_{10}H_{16}O_3$, limononic acid), *m/z* 199 ($C_{10}H_{16}O_4$, 7-hydroxy limononic acid) and *m/z* 245 ($C_{11}H_{18}O_6$).

Larger $C_{>20}$ products described by Kundu et al., (2012) and Bateman et al., (2009) could not be identified here. Since most products described in Kundu et al., (2012) are unsaturated, they would ultimately be oxidised in the conditions used here. It is also likely that the pre-concentration achieved by filter or impactor sampling in these studies leads to a greater sensitivity for species with very low concentrations compared to our online method.

Atmos. Chem. Phys. Discuss., doi:10.5194/acp-2017-186, 2017
Manuscript under review for journal Atmos. Chem. Phys.
Discussion started: 7 March 2017

Atmospheric Chemistry and Physics Discussions

We show time series for selected ions, along with the cumulative total ion current (TIC) across all ions, in Figure 5(b). The time resolution of the measurements is 4 minutes, which are shown as continuous lines for clarity. The EESI-MS ion source is stable over the > 4 hour time period of the experiment with respect both to the TIC and individual ion time series, demonstrating that the technique can operate continuously throughout long laboratory experiments.

As demonstrated in Gallimore and Kalberer (2013) and Gallimore et al., (submitted), relative intensity changes in EESI-MS can be used to infer relative concentration changes in the particle phase. Many individual time series scale approximately with the loss-corrected particle mass (Figure 3) as shown in Figure 5(b). Slightly different upward (e.g. *m/z* 201) or downward (e.g. *m/z* 215) trends can be observed as aging continues on longer timescales. This suggests a slow production or loss from multi-generational chemistry either in the gas or particle phases.

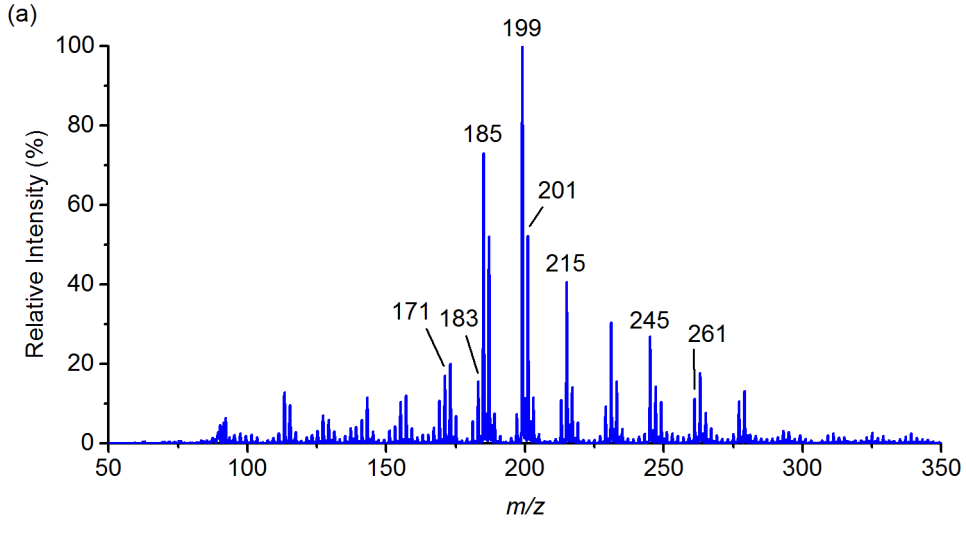

Atmos. Chem. Phys. Discuss., doi:10.5194/acp-2017-186, 2017
Manuscript under review for journal Atmos. Chem. Phys.
Discussion started: 7 March 2017

Atmospheric Chemistry and Physics Discussions

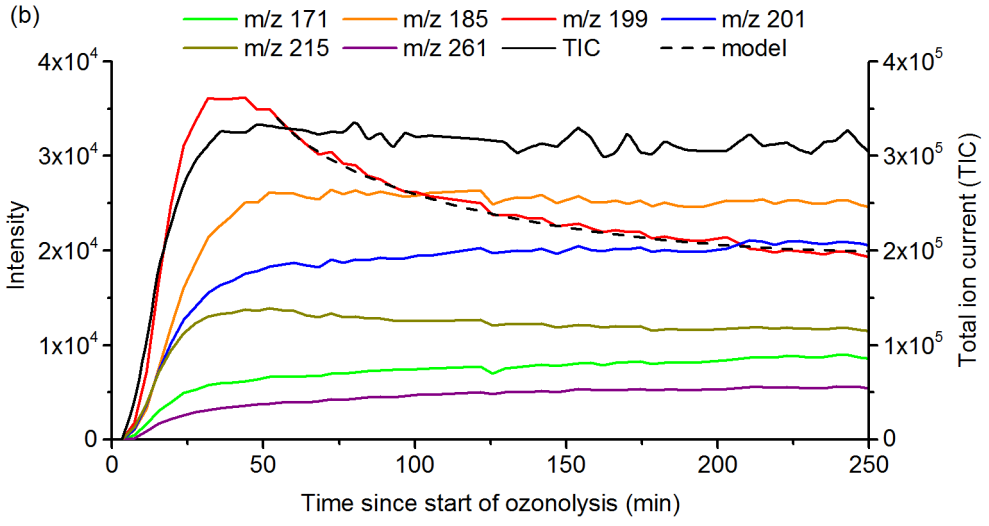

Figure 5: (a) EESI mass spectrum after 50 minutes. Some major peaks discussed in the text are labelled with their *m/z*. (b) Wall-loss corrected intensities for selected particle-phase ions detected using EESI-MS during limonene SOA formation. The total ion current (TIC) across the entire MS is shown on the secondary y-axis. The dashed line is a PG-AM simulation for the heterogeneous ozonolysis of unsaturated $C_{10}H_{16}O_4$ assuming semisolid SOA.

A number of ions over a large molecular weight range (*m/z* 107-295) deviate significantly from the above trend and become depleted from the aerosol on longer timescales. We focus on the most abundant of these, *m/z* 199 (Figure 5(b)) which peaks after ~ 30 minutes and then decays notably over the remainder of the experiment. Other ions showing similar trends are discussed later in section 3.2.

A few assignments exist for *m/z* 199 (neutral formula $C_{10}H_{16}O_4$), which has been observed as a major product in previous studies (Kundu et al., 2012; Walser et al., 2008). The most direct route to such an oxidised C_{10} species involves ring-opening by ozonolysis of the endo C=C and hence preservation of the intact carbon backbone. For instance, 7-hydroxy limononic acid is a compelling assignment which is functionalised at the former endo C=C and still contains an intact exo C=C. Other less direct formation routes may include reactive uptake of small carbonyls with $C_{<10}$ products in the particle phase, or (unsaturated) hydroperoxide formation (Kundu et al., 2012). We note that most plausible assignments for *m/z* 199 are unsaturated. The chemical loss of these species is therefore likely to include ozonolysis reactions. We propose that this is via heterogeneous reaction due to the low

volatility of any possible $C_{10}H_{16}O_4$ product. The very low corresponding gas phase signal (*m/z* 201, $[M + H]^+$) appears to confirm this.

Zhang et al., (2006) point out that for uptake coefficients (~ 10^{-3}) typical of other model SOA systems such as oleic acid, the heterogeneous loss rate of these species should be fast, and limited by their formation rate. By contrast, the characteristic time for loss of *m/z* 199 in this experiment is finite and relatively long, on the order of 1 hour. This is consistent with the study of Bateman et al., (2009), who found a ~ 30 minute lifetime for similar species (with higher ozone concentrations, ~ 1 ppm) using a time resolved analysis technique. Based on this slow loss, they estimated an effective ozonolysis rate coefficient of 10^3-10^4 M^{-1} s^{-1}, consistent with some rate constants measured in water (Hoigne and Bader, 1983) but 2-3 orders of magnitude lower than for a commonly used model SOA system, oleic acid (Lisitsyn et al., 2004).

We investigate this time dependence further, considering two possible scenarios: loss limited by bulk ozone-alkene reaction, and the formation of high viscosity particles which impede (an otherwise fast) bulk reaction. The latter of these has received substantial attention in recent years since the discovery that monoterpene-derived SOA can form an amorphous phase state (Virtanen et al., 2010). The characteristic time for bulk diffusion described in Shiraiwa et al., (2011) is on the order of minutes-hours for a semisolid accumulation mode particle, consistent with the 30-60 minutes estimated here and in Bateman et al., (2009).

The two scenarios were modelled by simulating reactive uptake of ozone to SOA containing unsaturated $C_{10}H_{16}O_4$ using the Pretty Good Aerosol Model (PG-AM, (Griffiths et al., 2009), (Gallimore et al., submitted)). The model was initialised to the experimental conditions 50 minutes after the introduction of ozone; an initial mole fraction of 0.05 was assumed for unsaturated $C_{10}H_{16}O_4$ based on the ion intensities in Figure 5(a) and further production was neglected. Physico-chemical model parameters were fixed (section 2.5), with the exception of the organic and oxidant diffusion coefficients, and ozonolysis rate constant, which were varied manually.

Atmos. Chem. Phys. Discuss., doi:10.5194/acp-2017-186, 2017
Manuscript under review for journal Atmos. Chem. Phys.
Discussion started: 7 March 2017

Atmospheric Chemistry and Physics Discussions

In the bulk diffusion-limited scenario, an ozonolysis rate constant of k^{II} = 10^{6} M^{-1} s^{-1}, comparable to oleic acid, was assumed. To reproduce our observations, diffusion coefficients representative of semisolid SOA were required. The model simulation overlaid on Figure 5(b) is for D_{org} = 10^{-16} and D_{O3} = 5 × 10^{-9} cm^2 s^{-1} respectively. The model was found to be sensitive to both parameters and various combinations in the range D_{org} = 10^{-15}-10^{-17} and D_{O3} = 10^{-7}-10^{-9} cm^2 s^{-1} provide reasonable fits to the data.

For the bulk reaction-limited scenario, the modelled concentration was sensitive only to the slow bulk ozonolysis rate constant, k^{II}, for any representative liquid SOA diffusion coefficients (D_{O3} > 10^{-6} and D_{org} > 10^{-10} cm^2 s^{-1} respectively). k^{II} = 8 × 10^{3} M^{-1} s^{-1} was found to give the best agreement with our measurements, in good agreement with the range (10^{3}-10^{4} M^{-1} s^{-1}) estimated by Bateman et al., (2009). The modelled decay profile was very similar to the diffusion-limited case and so is omitted from Figure 5(b) for clarity.

The extent to which high particle viscosity influences reactivity is still an open question and we are not aware of any studies of the viscosity properties of limonene SOA. However, the diffusion coefficients used here are at the lower limit of what has been reported for monoterpene SOA at 40% RH (Renbaum-Wolff et al., 2013) (D_{org} ≥ 10^{-16} cm^2 s^{-1}) and significantly lower than some other determinations in SOA, e.g. (Hosny et al., 2016) (D_{org} ~ 10^{-11} cm^2 s^{-1}). It therefore seems unlikely that the aerosol is sufficiently viscous to fully explain our data, but a combination of slow diffusion and reaction may well do, especially given further suggestions of inhibited reactivity discussed in the following section. A more detailed modelling investigation is out of the scope of this study given the lack of constraining experimental data (both here and in general for limonene SOA) and the assumptions made about the chemical identity of *m/z* 199. However, this prompts further study of the diffusion characteristics of limonene SOA, especially since the SOA yield is higher and the aerosol components more oxidised than for many other biogenic VOCs.

Atmos. Chem. Phys. Discuss., doi:10.5194/acp-2017-186, 2017
Manuscript under review for journal Atmos. Chem. Phys.
Discussion started: 7 March 2017

Atmospheric Chemistry and Physics Discussions

3.2 Particle-bound Reactive Oxygen Species (ROS) quantification

We also monitored the formation of particle-bound reactive oxygen species (ROS) during the chamber experiment. We report ROS quantities as an equivalent concentration of hydrogen peroxide per cubic metre of air which reflects the effective reactivity of the ROS present in the aerosol to the assay (red curve in Figure 6). The appearance of ROS is highly correlated in time with the formation of SOA mass in the chamber (Figure 3) within the first few minutes of ozone introduction. However, while the SOA mass concentration continues to increase slowly for a number of hours, the ROS signal reaches a small maximum after around 30 minutes. Both tend towards relatively stable values after the first hour of oxidative chemistry in the chamber, consistent with the relatively small composition changes in the aerosol (Figure 5(b)). To make this more explicit, we normalise this measured quantity to the mass of SOA present to give a relative in-particle concentration (blue curve in Figure 6). The mass-weighted ROS concentration is highest in the early stages of the reaction, before tending to a stable value of 0.42 ± 0.04 nmol $[H_2O_2]$ μg^{-1} after the first hour of the experiment.

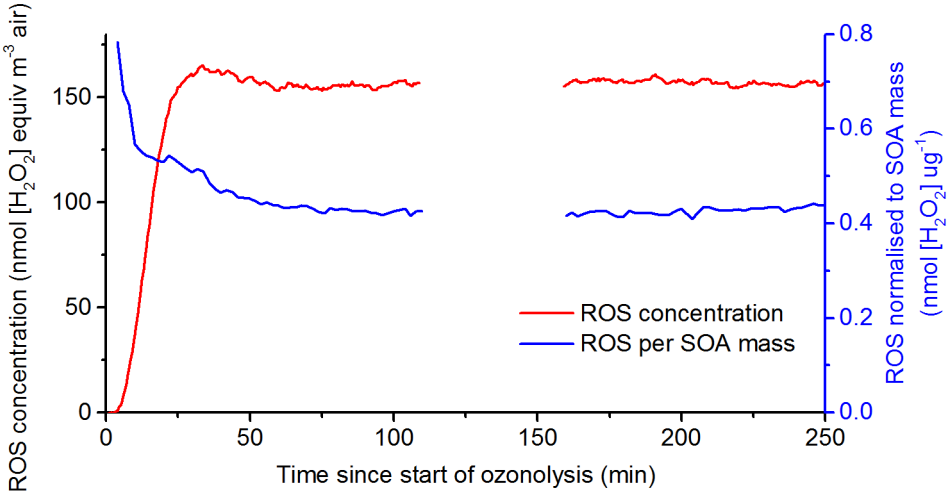

Figure 6: Wall loss corrected particle-bound ROS detected using OPROSI during limonene SOA formation. The procedural blank at 110-160 minutes has been removed for clarity. The secondary y-axis shows an effective ROS concentration per mass of aerosol, which is highest at the start of the experiment and reaches a stable value of 0.42 ± 0.04 nmol $[H_2O_2]$ per µg SOA.

Atmos. Chem. Phys. Discuss., doi:10.5194/acp-2017-186, 2017
Manuscript under review for journal Atmos. Chem. Phys.
Discussion started: 7 March 2017

Atmospheric Chemistry and Physics Discussions

We present an analysis of the above time series which proposes that the total ROS signal can be decomposed in to two components with different characteristic lifetimes:

$$[ROS_{total}] = [ROS_{long}] + [ROS_{short}] \quad \textbf{(1)}$$

We propose that ROS_{long} are a group of relatively stable long-lived products (such as organic peroxides) which constitute the stable ROS at the end of the experiment, and ROS_{short} are reactive species (possibly radicals or otherwise short-lived compounds such as reactive peroxides) species which are produced directly from ozonolysis or other early-generation reactions. Previous studies have concluded that a substantial fraction of ROS present in laboratory (Fuller et al., 2014) and ambient (Huang et al., 2016) aerosols is short lived.

If we assume that $[ROS_{long}]$ scales with the total particle mass in proportion to the final mass-weighted ROS concentration (as do most individual aerosol components in Figure 5(b)), the net contribution of $[ROS_{short}]$ to the total measured signal can be estimated:

$$[ROS_{total}] = 0.42 \times Mass_{SOA} + [ROS_{short}] \quad \textbf{(2)}$$

Figure 7(a) shows the estimated contributions of long- and short-lived ROS to the total measured ROS signal using Equation 2. Based on this simple analysis, long-lived ROS makes the dominant contribution to the total ROS signal over the course of the experiment. As expected from the mass-weighted ROS curve in Figure 6, short-lived ROS is most important early in the reaction when reactive species are being produced by ozonolysis from the limonene precursor (Figure 4).

Atmos. Chem. Phys. Discuss., doi:10.5194/acp-2017-186, 2017
Manuscript under review for journal Atmos. Chem. Phys.
Discussion started: 7 March 2017

Atmospheric Chemistry and Physics Discussions

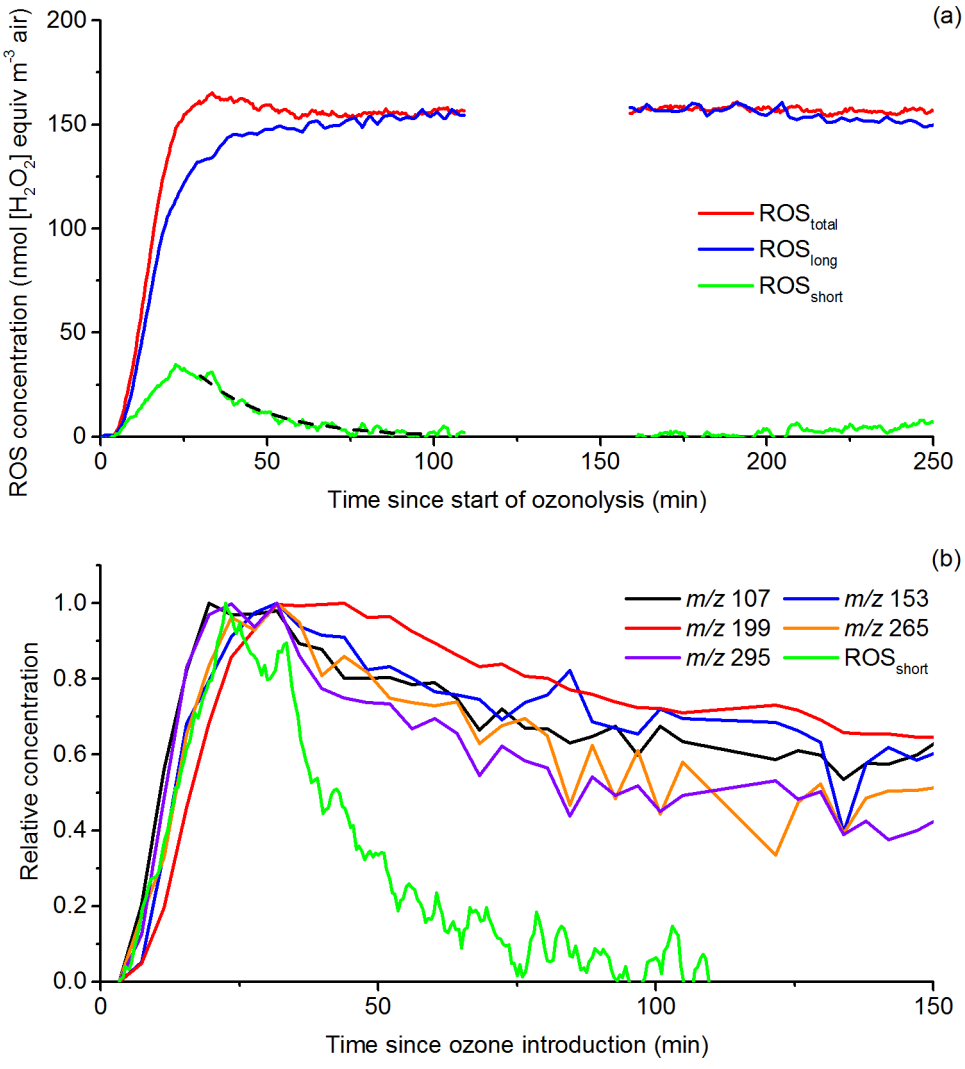

Figure 7: (a) Total particle-bound ROS decomposed into short-lived and long-lived components according to Equation 2. The black dashed line represents an exponential fit to ROS_{short} with a characteristic lifetime of 17 minutes. (b) Relative abundance of a number of particle-phase ions which decay substantially over the course of the experiment. It is possible that some of these contain tracers for ROS_{short} (green curve) if the total ion intensities are a combination of short-lived and stable species.

Atmos. Chem. Phys. Discuss., doi:10.5194/acp-2017-186, 2017
Manuscript under review for journal Atmos. Chem. Phys.
Discussion started: 7 March 2017

[ROS_{short}] reaches a maximum around 20 minutes into the experiment and tends towards zero at longer times. This reflects the competition between production and loss for short-lived species. The apparent production rate of ROS_{short} will depend on two factors. Firstly, chemical production (likely predominantly in the gas phase, but also via heterogeneous ozonolysis of later generation products), which will be fastest at the start of ozonolysis when precursor concentrations are at their highest. Secondly, gas-particle partitioning of reactive species, which will increasingly favour the particle phase as the mass loading in the chamber increases. A convolution of these factors is a plausible explanation for the maximum in [ROS_{short}] in Figure 7(a). At longer times, where the concentration of organic radical precursors (e.g. limonene) is reduced, chemical loss of ROS_{short} dominates and by definition in Equation 2 tends to zero at longer times.

We estimate the lifetime of particle-bound ROS_{short} by neglecting further production of short-lived species after 30 minutes, since the rate of change of chemical composition (Figures 4 and 5) and particle mass (Figure 3) has slowed by this point. We note that the 4 minute time resolution of the instrument (determined mainly by mixing times in the particle collector and fluorescence detector cell) will act as a lower limit on the apparent ROS_{short} lifetime in this analysis. The black dashed curve in Figure 7(a) represents an exponential fit to the data between 30 and 110 minutes and yields a characteristic time for pseudo first-order ROS_{short} loss of 17 minutes. This may be a overestimate if ROS_{short} production is not negligible during this time. Equation 2 also neglects any possible secondary chemistry involved in forming long-lived ROS.

We have interrogated the EESI-MS data for species which may act as tracers for ROS_{short} based on their time dependence. As mentioned above, in addition to *m/z* 199, a number of other ions (over the range *m/z* 107-295) show a characteristic maximum at early times in the reaction followed by notable decay over the remainder of the experiment (Figure 7(b)). All of these ions could contain enough oxygen atoms to possess ROS-active functional groups, although we do not obtain definitive molecular formulae. While none of these ion time series map perfectly onto the ROS_{short} data, several species may be present for each low resolution peak such that the loss of some ROS compounds is obscured by others with different time

dependences. Given the hints that ROS tracers could be present, and recent progress in the MS detection of peroxides (Steimer et al., 2017), more definitive identification of ROS-active compounds via EESI-MS may be possible in future.

Qualitatively, the ROS observations in the current study compare well with Fuller et al., (2014) who noted that oxidised oleic acid aerosols contained both short- and long-lived ROS components using the same assay. The quantitative differences are summarised in Table 2. In summary, limonene ROS was formed in overall higher yield and the short-lived components were in general longer lived. These differences can be rationalised by considering the molecular properties of oleic acid and limonene.

	Limonene SOA (this study)	Oleic acid SOA (Fuller et al., 2014)
ROS_{long} yield (nmol $[H_2O_2]$ μg^{-1})	0.42	0.14
Maximum fraction of ROS_{short} (%)	25-40	75
ROS_{short} lifetime (mins)	17	a few

Table 2: Quantitative differences in ROS formation between the current study (limonene SOA) and Fuller et al., (2014) (oleic acid SOA). More long-lived ROS is formed for limonene, but short-lived ROS appears more important for oleic acid.

The majority (~75 %) of ROS detected for freshly oxidised oleic acid particles was short-lived in nature, compared to a relatively smaller fraction for limonene SOA in the current study. Oleic acid is of low volatility and subject only to heterogeneous ozonolysis in the particle, so ROS production will be in-situ in the particle phase. As discussed above, the oxidation of limonene is a more complex multiphase process, and at least initially a large fraction of organic intermediates will be produced in the gas-phase. Since such species have short gas-phase lifetimes, many will go on to react further (e.g. to make long-lived ROS by reaction with water (Docherty et al., 2005)) before entering the particle phase, leading to an overall different ratio of short- and long-lived ROS in the oleic acid and limonene-SOA particles.

Atmos. Chem. Phys. Discuss., doi:10.5194/acp-2017-186, 2017
Manuscript under review for journal Atmos. Chem. Phys.
Discussion started: 7 March 2017

The overall yield of ROS_{long} is higher for limonene by a factor of 3. Limonene contains two C=C, and therefore more potential to form highly oxygenated products (including ROS) than oleic acid with a single C=C. As discussed above, the fates of initial products may also be different as a result of the reaction phase and the presence of water vapour in the current experiments.

Finally, the ROS_{short} lifetime in Fuller et al., (2014) was shorter (a few minutes) than that reported here (17 minutes). We note that the oleic acid data were collected in an offline manner which decoupled ROS_{short} production and loss. This is not possible for online sampling and as discussed above this could result in an overestimated ROS_{short} lifetime for limonene SOA. Particle viscosity may also play a role: oleic acid remains liquid throughout ozonolysis (Hosny et al., 2016) and so in-particle reactions which consume ROS_{short} should not be inhibited. If limonene SOA were viscous, as considered above, this could extend the effective lifetime of short lived species.

The very recent study of Tuet et al., (2017) also found that the oxidative potential of SOA, quantified using a different assay, depends on the hydrocarbon precursor. Particularly high redox activity was found for naphthalene-derived SOA. However, comparing directly between different assays is challenging because the relative sensitivity towards different organic components (e.g. peroxides, quinones, radicals, polyaromatic hydrocarbons) is not well established (Fang et al., 2015).

4 Conclusions

The new 5.4 m^3 Cambridge Atmospheric Simulation Chamber (CASC) facility enables atmospheric chemical processes to be studied in the laboratory under relevant conditions with a high degree of time and chemical resolution. The characteristics of the chamber in terms of lights, mixing and wall losses have been thoroughly characterised as an important benchmark for current and future studies. The multiphase oxidation of limonene was studied using a range of continuous time-resolved particle and gas-phase measurements. The merits of highly

time resolved measurements of particle composition and reactive oxygen species (ROS) were demonstrated and the links between the two explored for limonene SOA.

The majority of particle bound ROS detected in limonene SOA is long lived on the experiment timescale (4 hours) suggesting an important role for such health-relevant species in ambient particles. The overall yield of ROS was also significantly higher than for another SOA model system studied with the same methodology, oleic acid. This may have important implications for indoor air quality in particular given the abundance of limonene in cleaning and "air freshening" products. Even for relatively simple model SOA systems, the time-dependent characteristics of ROS are variable and reflect the underlying chemistry of the gas and particle phases in terms of reactivity, partitioning and viscosity.

The apparently slow loss of unsaturated species via heterogeneous ozonolysis, and the relatively long decay time of ROS_{short}, both provide indirect evidence of a role for viscous particle formation in limonene SOA. We note that substantial uncertainties remain associated with in-particle diffusion and gas-particle exchange in viscous organic aerosols. However, if particle viscosity is impeding chemical reactivity, these particles are in essence a reservoir for reactive organics (both unsaturated and health-relevant). Such reactive carbon may therefore enjoy an extended lifetime in the atmosphere before reacting in more humid regions, or in particular the elevated RH and temperature conditions of the human airways. The potential atmospheric and health implications of this hypothesis merit further study for limonene SOA and other aerosol systems.

Supplementary information

Chamber characterisation data relating to the spectra of the light sources, the mixing of VOCs, and particle wall loss rates are provided.

Acknowledgements

This work was funded by the European Research Council (grant 279405), the UK Natural Environment Research Council (grant NE/H52449X/1) and the Velux foundation (project number 593).

Data access

Data presented in this study can be obtained by contacting the corresponding author.

References

Abbatt, J. P. D., Lee, A. K. Y. and Thornton, J. A.: Quantifying trace gas uptake to tropospheric aerosol: recent advances and remaining challenges., Chem. Soc. Rev., 41(19), 6555–81, doi:10.1039/c2cs35052a, 2012.

Bateman, A. P., Nizkorodov, S. A., Laskin, J. and Laskin, A.: Time-resolved molecular characterization of limonene/ozone aerosol using high-resolution electrospray ionization mass spectrometry, Phys. Chem. Chem. Phys., 11(36), 7931–7942, doi:10.1039/b916865f, 2009.

Blake, R. S., Monks, P. S. and Ellis, A. M.: Proton-transfer reaction mass spectrometry., Chem. Rev., 109(3), 861–96, doi:10.1021/cr800364q, 2009.

Boucher, O., Randall, D., Artaxo, P., Bretherton, C., Feingold, G., Forster, P., Kerminen, V.-M., Kondo, Y., Liao, H., Lohmann, U., Rasch, P., Satheesh, S. K., Sherwood, S., Stevens, B. and Zhang, X. Y.: Clouds and Aerosols, in Climate Change 2013: The Physical Science Basis. Contribution of Working Group I to the Fifth Assessment Report of the Intergovernmental Panel on Climate Change, edited by T. F. Stocker, D. Qin, G.-K. Plattner, M. Tignor, S. K. Allen, J. Boschung, A. Nauels, Y. Xia, V. Bex, and P. M. Midgley., 2013.

Cocker, D. R., Flagan, R. C. and Seinfeld, J. H.: State-of-the-art chamber facility for studying atmospheric aerosol chemistry, Environ. Sci. Technol., 35(12), 2594–2601, doi:10.1021/es0019169, 2001.

Docherty, K. S., Wu, W., Lim, Y. Bin and Ziemann, P. J.: Contributions of organic peroxides to secondary aerosol formed from reactions of monoterpenes with O3, Environ. Sci. Technol., 39(11), 4049–4059, doi:10.1021/es050228s, 2005.

Donahue, N. M., Tischuk, J. E., Marquis, B. J. and Huff Hartz, K. E.: Secondary organic aerosol from limona ketone: insights into terpene ozonolysis via synthesis of key intermediates, Phys. Chem. Chem. Phys., 9(23), 2991–2998, doi:10.1039/B701333G, 2007.

Ehn, M., Thornton, J. A., Kleist, E., Sipilä, M., Junninen, H., Pullinen, I., Springer, M., Rubach, F., Tillmann, R., Lee, B., Lopez-Hilfiker, F., Andres, S., Acir, I.-H., Rissanen, M., Jokinen, T.,

Schobesberger, S., Kangasluoma, J., Kontkanen, J., Nieminen, T., Kurtén, T., Nielsen, L. B., Jørgensen, S., Kjaergaard, H. G., Canagaratna, M., Maso, M. D., Berndt, T., Petäjä, T., Wahner, A., Kerminen, V.-M., Kulmala, M., Worsnop, D. R., Wildt, J. and Mentel, T. F.: A large source of low-volatility secondary organic aerosol, Nature, 506(7489), 476–9, doi:10.1038/nature13032, 2014.

Ervens, B., Turpin, B. J., Weber, R. J., Brunswick, N. and Sciences, A.: Secondary organic aerosol formation in cloud droplets and aqueous particles (aqSOA): A review of laboratory, field and model studies, Atmos. Chem. Phys., 11(21), 11069–11102, doi:10.5194/acp-11-11069-2011, 2011.

Fang, T., Verma, V., Guo, H., King, L. E., Edgerton, E. S. and Weber, R. J.: A semi-automated system for quantifying the oxidative potential of ambient particles in aqueous extracts using the dithiothreitol (DTT) assay : results from the Southeastern Center for Air Pollution and Epidemiology (SCAPE), Atmos. Meas. Tech., 8, 471–482, doi:10.5194/amt-8-471-2015, 2015.

Fuller, S. J., Wragg, F. P. H., Nutter, J. and Kalberer, M.: Comparison of on-line and off-line methods to quantify reactive oxygen species (ROS) in atmospheric aerosols, Atmos. Environ., 92, 97–103, doi:10.1016/j.atmosenv.2014.04.006, 2014.

Gallimore, P. J. and Kalberer, M.: Characterizing an extractive electrospray ionization (EESI) source for the online mass spectrometry analysis of organic aerosols, Environ. Sci. Technol., 47(13), 7324–31, doi:10.1021/es305199h, 2013.

Gallimore, P.J., Griffiths, P.T., Pope, F.D., Reid, J.P. and Kalberer, M.: Comprehensive modelling study of ozonolysis of oleic acid aerosol based on real-time, online measurements of aerosol composition, J. Geophys. Res.: Atmos., submitted.

de Gouw, J. and Warneke, C.: Measurements of volatile organic compounds in the earth's atmosphere using proton-transfer-reaction mass spectrometry, Mass Spectrom. Rev., 26(2), 223–57, doi:10.1002/mas.20119, 2007.

Griffiths, P. T., Badger, C. L., Cox, R. A., Folkers, M., Henk, H. H. and Mentel, T. F.: Reactive uptake of N2O5 by aerosols containing dicarboxylic acids. Effect of particle phase, composition, and nitrate content, J. Phys. Chem. A, 113(17), 5082–5090, doi:10.1021/jp8096814, 2009.

Guenther, A., Geron, C., Pierce, T., Lamb, B., Harley, P. and Fall, R.: Natural emissions of non-methane volatile organic compounds, carbon monoxide, and oxides of nitrogen from North America, Atmos. Environ., 34(12–14), 2205–2230, doi:10.1016/S1352-2310(99)00465-3, 2000.

Hallquist, M., Wenger, J. C., Baltensperger, U., Rudich, Y., Simpson, D., Claeys, M., Dommen, J., Donahue, N. M., George, C., Goldstein, A. H., Hamilton, J. F., Herrmann, H., Hoffmann, T., Iinuma, Y., Jang, M., Jenkin, M. E., Jimenez, J. L., Kiendler-Scharr, A., Maenhaut, W., McFiggans, G., Mentel, T. F., Monod, A., Prévôt, A. S. H., Seinfeld, J. H., Surratt, J. D., Szmigielski, R. and Wildt, J.: The formation, properties and impact of secondary organic aerosol: current and emerging issues, Atmos. Chem. Phys., 9, 5155–5236, 2009.

den Hartigh, L. J., Lamé, M. W., Ham, W., Kleeman, M. J., Tablin, F. and Wilson, D. W.: Endotoxin and polycyclic aromatic hydrocarbons in ambient fine particulate matter from Fresno, California initiate human monocyte inflammatory responses mediated by reactive oxygen species, Toxicol. Vitr., 24(7), 1993–2002, doi:10.1016/j.tiv.2010.08.017, 2010.

Hildebrandt, L., Donahue, N. M. and Pandis, S. N.: High formation of secondary organic aerosol from the photo-oxidation of toluene, Atmos. Chem. Phys., 9(9), 2973–2986, doi:10.5194/acp-9-2973-2009,

2009.

Hoffmann, T., Odum, J. R., Bowman, F., Collins, D., Klockow, D., Flagan, R. C. and Seinfeld, J. H.: Formation of organic aerosols from the oxidation of biogenic hydrocarbons, J. Atmos. Chem., 26(2), 189–222, doi:10.1023/A:1005734301837, 1997.

Hoigne, J. and Bader, H.: Rate Constants of Reactions of Ozone with Organic and Inorganic Compounds in Water - I: Non-Dissociating Organic Compounds, Water Res., 17, 173–183, 1983.

Hosny, N. A., Fitzgerald, C., Vysniauskas, A., Athanasiadis, T., Berkemeier, T., Uygur, N., Pöschl, U., Shiraiwa, M., Kalberer, M., Pope, F. D. and Kuimova, M. K.: Direct imaging of changes in aerosol particle viscosity upon hydration and chemical aging, Chem. Sci., 7, 1357–1367, doi:10.1039/C5SC02959G, 2016.

Huang, W., Zhang, Y., Zhang, Y., Zeng, L., Dong, H., Huo, P., Fang, D. and Schauer, J. J.: Development of an automated sampling-analysis system for simultaneous measurement of reactive oxygen species (ROS) in gas and particle phases: GAC-ROS, Atmos. Environ., 134, 18–26, doi:10.1016/j.atmosenv.2016.03.038, 2016.

Ishizuka, Y., Tokumura, M., Mizukoshi, A., Noguchi, M. and Yanagisawa, Y.: Measurement of secondary products during oxidation reactions of terpenes and ozone based on the PTR-MS analysis: Effects of coexistent carbonyl compounds, Int. J. Environ. Res. Public Health, 7(11), 3853–3870, doi:10.3390/ijerph7113853, 2010.

Kalberer, M., Paulsen, D., Sax, M., Steinbacher, M., Dommen, J., Prevot, A. S. H., Fisseha, R., Weingartner, E., Frankevich, V., Zenobi, R. and Baltensperger, U.: Identification of polymers as major components of atmospheric organic aerosols., Science (80-.)., 303(5664), 1659–1662, doi:10.1126/science.1092185, 2004.

Klotz, B., Sørensen, S., Barnes, I., Becker, K. H., Etzkorn, T., Volkamer, R., Platt, U., Wirtz, K. and Martın-Reviejo, M.: Atmospheric Oxidation of Toluene in a Large-Volume Outdoor Photoreactor: In Situ Determination of Ring-Retaining Product Yields, J. Phys. Chem. A, 102, 10289–10299, doi:10.1021/jp982719n, 1998.

Kourtchev, I., Giorio, C., Manninen, A., Wilson, E., Mahon, B., Aalto, J., Kajos, M., Venables, D., Ruuskanen, T., Levula, J., Mentel, T., Rudich, Y., Hallquist, M., Doussin, J.-F., Maenhaut, W., Jaana, B., Petäjä, T., Wenger, J., Kulmala, M. and Kalberer, M.: Enhanced Volatile Organic Compounds emissions and organic aerosol mass increase the oligomer content of atmospheric aerosols, Sci. Rep., (October), 1–9, doi:10.1038/srep35038, 2016.

Kroll, J. H. and Seinfeld, J. H.: Chemistry of secondary organic aerosol: Formation and evolution of low-volatility organics in the atmosphere, Atmos. Environ., 42(16), 3593–3624, doi:10.1016/j.atmosenv.2008.01.003, 2008.

Kundu, S., Fisseha, R., Putman, A. L., Rahn, T. A. and Mazzoleni, L. R.: High molecular weight SOA formation during limonene ozonolysis: Insights from ultrahigh-resolution FT-ICR mass spectrometry characterization, Atmos. Chem. Phys., 12(12), 5523–5536, doi:10.5194/acp-12-5523-2012, 2012.

Lee, A., Goldstein, A. H., Keywood, M. D., Gao, S., Varutbangkul, V., Bahreini, R., Ng, N. L., Flagan, R. C. and Seinfeld, J. H.: Gas-phase products and secondary aerosol yields from the ozonolysis of ten different terpenes, J. Geophys. Res., 111(D7), D07302, doi:10.1029/2005JD006437, 2006.

Lisitsyn, D. M., Razumovskii, S. D., Tishenin, M. A. and Titov, V. N.: Kinetic parameters of oxidation of individual fatty acids with ozone, Bull. Exp. Biol. Med., 138(5), 457–459, doi:10.1007/s10517-005-0069-9, 2004.

Martın-Reviejo, M. and Wirtz, K.: Is Benzene a Precursor for Secondary Organic Aerosol ?, Environ. Sci. Technol., 39, 1045–1054, 2005.

McNeill, V. F., Woo, J. L., Kim, D. D., Schwier, A. N., Wannell, N. J., Sumner, A. J. and Barakat, J. M.: Aqueous-phase secondary organic aerosol and organosulfate formation in atmospheric aerosols: A modeling study, Environ. Sci. Technol., 46, 8075–8081, doi:10.1021/es3002986, 2012.

Morris, J. W., Davidovits, P., Jayne, J. T., Jimenez, J. L., Shi, Q., Kolb, C. E. and Worsnop, D. R.: Kinetics of submicron oleic acid aerosols with ozone : A novel aerosol mass spectrometric technique, , 29(9), 3–6, 2002.

Odum, J. R., Jungkamp, T. P. ., Griffin, R. J., Flagan, R. C. and Seinfeld, J. H.: The Atmospheric Aerosol-Forming Potential of Whole Gasoline Vapor, Science (80-.)., 39, 96–99, 1997.

Paulsen, D., Dommen, J., Kalberer, M., Prévôt, A. S. H., Richter, R., Sax, M., Steinbacher, M., Weingartner, E. and Baltensperger, U.: Secondary organic aerosol formation by irradiation of 1,3,5-trimethylbenzene-NOx-H2O in a new reaction chamber for atmospheric chemistry and physics., Environ. Sci. Technol., 39(8), 2668–2678, doi:10.1021/es0489137, 2005.

Pope, C. A., Ezzati, M. and Dockery, D. W.: Fine-particulate air pollution and life expectancy in the United States, N. Engl. J. Med., 360(4), 376–86, doi:10.1056/NEJMsa0805646, 2009.

Renbaum-Wolff, L., Grayson, J. W., Bateman, A. P., Kuwata, M., Sellier, M., Murray, B. J., Shilling, J. E., Martin, S. T. and Bertram, A. K.: Viscosity of α-pinene secondary organic material and implications for particle growth and reactivity., Proc. Natl. Acad. Sci. U. S. A., 110(20), 8014–9, doi:10.1073/pnas.1219548110, 2013.

Rohrer, F., Bohn, B., Brauers, T., Brüning, D., Johnen, F.-J., Wahner, a. and Kleffmann, J.: Characterisation of the photolytic HONO-source in the atmosphere simulation chamber SAPHIR, Atmos. Chem. Phys. Discuss., 4(6), 7881–7915, doi:10.5194/acpd-4-7881-2004, 2004.

Rollins, A. W., Kiendler-Scharr, A., Fry, J. L., Brauers, T., Brown, S. S., Dorn, H.-P., Dubé, W. P., Fuchs, H., Mensah, A., Mentel, T. F., Rohrer, F., Tillmann, R., Wegener, R., Wooldridge, P. J., Cohen, R. C., Tilmann, R., Wegener, R., Wooldridge, P. J. and Cohen, R. C.: Isoprene oxidation by nitrate radical: alkyl nitrate and secondary organic aerosol yields, Atmos. Chem. Phys., 9(2), 6685–6703, doi:10.5194/acpd-9-8857-2009, 2009.

Shiraiwa, M., Ammann, M., Koop, T. and Pöschl, U.: Gas uptake and chemical aging of semisolid organic aerosol particles., Proc. Natl. Acad. Sci. U. S. A., 108(27), 11003–11008, doi:10.1073/pnas.1103045108, 2011.

Shiraiwa, M., Yee, L. D., Schilling, K. a, Loza, C. L., Craven, J. S., Zuend, A., Ziemann, P. J. and Seinfeld, J. H.: Size distribution dynamics reveal particle-phase chemistry in organic aerosol formation, Proc. Natl. Acad. Sci. U. S. A., 110(29), 11746–50, doi:10.1073/pnas.1307501110, 2013.

Steenhof, M., Gosens, I., Strak, M., Godri, K. J., Hoek, G., Cassee, F. R., Mudway, I. S., Kelly, F. J., Harrison, R. M., Lebret, E., Brunekreef, B., Janssen, N. A. H. and Pieters, R. H. H.: In vitro toxicity of particulate matter (PM) collected at different sites in the Netherlands is associated with PM

composition, size fraction and oxidative potential--the RAPTES project., Part. Fibre Toxicol., 8, 26, doi:10.1186/1743-8977-8-26, 2011.

Steimer, S. S., Kourtchev, I. and Kalberer, M.: Mass Spectrometry Characterization of Peroxycarboxylic Acids as Proxies for Reactive Oxygen Species and Highly Oxygenated Molecules in Atmospheric Aerosols, Anal. Chem., in press, doi:10.1021/acs.analchem.6b04127, 2017.

Tuet, W. Y., Chen, Y., Xu, L., Fok, S., Gao, D., Weber, R. J. and Ng, N. L.: Chemical oxidative potential of secondary organic aerosol (SOA) generated from the photooxidation of biogenic and anthropogenic volatile organic compounds, Atmos. Chem. Phys., 17, 839–853, doi:10.5194/acp-17-839-2017, 2017.

Verma, V., Ning, Z., Cho, A. K., Schauer, J. J., Shafer, M. M. and Sioutas, C.: Redox activity of urban quasi-ultrafine particles from primary and secondary sources, Atmos. Environ., 43(40), 6360–6368, doi:10.1016/j.atmosenv.2009.09.019, 2009.

Virtanen, A., Joutsensaari, J., Koop, T., Kannosto, J., Yli-Pirilä, P., Leskinen, J., Mäkelä, J. M., Holopainen, J. K., Pöschl, U., Kulmala, M., Worsnop, D. R. and Laaksonen, A.: An amorphous solid state of biogenic secondary organic aerosol particles, Nature, 467(7317), 824–7, doi:10.1038/nature09455, 2010.

Wainman, T., Zhang, J., Weschler, C. J. and Lioy, P. J.: Ozone and Limonene in Indoor Air : A Source of Submicron Particle Exposure Author (s): Thomas Wainman , Junfeng Zhang , Charles J . Weschler and Paul J . Lioy Published by : The National Institute of Environmental Health Sciences Stable URL : http://www, Environ. Health Perspect., 108(12), 1139–1145, 2000.

Walser, M. L., Desyaterik, Y., Laskin, J., Laskin, A. and Nizkorodov, S. A.: High-resolution mass spectrometric analysis of secondary organic aerosol produced by ozonation of limonene., Phys. Chem. Chem. Phys., 10(7), 1009–1022, doi:10.1039/B712620D, 2008.

Wang, X., Liu, T., Bernard, F., Ding, X., Wen, S., Zhang, Y., Zhang, Z., He, Q., Lu, S., Chen, J., Saunders, S., Yu, J., Lü, S. and Chen, J.: Design and characterization of a smog chamber for studying gas-phase chemical mechanisms and aerosol formation, Atmos. Meas. Tech., 7, 301–313, doi:10.5194/amt-7-301-2014, 2014.

Waring, M. S.: Secondary organic aerosol (SOA) formation by limonene ozonolysis: Parameterizing multi-generational chemistry in ozone- and residence time-limited indoor environments, Atmos. Environ., doi:10.1016/j.atmosenv.2016.08.051, 2016.

Weschler, C. J. and Shields, H. C.: Indoor ozone/terpene reactions as a source of indoor particles, Atmos. Environ., 33, 2301–2312, 1999.

Wragg, F. P. H., Fuller, S. J., Freshwater, R., Green, D. C., Kelly, F. J. and Kalberer, M.: An automated online instrument to quantify aerosol-bound reactive oxygen species (ROS) for ambient measurement and health-relevant aerosol studies, Atmos. Meas. Tech., 9, 4891–4900, doi:10.5194/amt-9-4891-2016, 2016.

Zhang, J., Huff Hartz, K. E., Pandis, S. N. and Donahue, N. M.: Secondary organic aerosol formation from limonene Ozonolysis: Homogeneous and heterogeneous influences as a function of NO x, J. Phys. Chem. A, 110, 11053–11063, doi:10.1021/jp062836f, 2006.

Zhao, J. and Zhang, R.: Proton transfer reaction rate constants between hydronium ion (H3O+) and

volatile organic compounds, Atmos. Environ., 38(14), 2177–2185, doi:10.1016/j.atmosenv.2004.01.019, 2004.